Applied Physics Letters

Effect of dipolar interaction on exceptional points in synthetic layered magnets

Cite as: Appl. Phys. Lett. **118**, 202401 (2021); https://doi.org/10.1063/5.0049011
Submitted: 28 February 2021 • Accepted: 26 April 2021 • Published Online: 17 May 2021

T. Jeffrey, W. Zhang and J. Sklenar

AIP Publishing

Applied Physics Letters ARTICLE scitation.org/journal/apl

Effect of dipolar interaction on exceptional points in synthetic layered magnets

Cite as: Appl. Phys. Lett. **118**, 202401 (2021); doi: 10.1063/5.0049011
Submitted: 28 February 2021 · Accepted: 26 April 2021 ·
Published Online: 17 May 2021

T. Jeffrey,[1] W. Zhang,[2] and J. Sklenar[1,a)]

AFFILIATIONS

[1]Department of Physics and Astronomy, Wayne State University, Detroit, Michigan 48202, USA
[2]Department of Physics, Oakland University, Rochster, Michigan 48309, USA

Note: This paper is part of the APL Special Collection on Mesoscopic Magnetic Systems: From Fundamental Properties to Devices.
[a)]**Author to whom correspondence should be addressed:** jnsklenar@wayne.edu

ABSTRACT

Within both synthetic ferromagnets and antiferromagnets, exceptional points, where optical and acoustic magnons coalesce into a single branch, can be used to control the magnon energy spectra. To date, exceptional point phenomena in magnon systems have been predominantly predicted and understood within the framework of macrospin models that are based upon coupled Landau–Lifshitz–Gilbert equations of motion. Although these equations can be readily linearized and solved, they do not necessarily incorporate all of the physical effects that are present in a real synthetic magnetic structure such as dipolar interactions. We have used micromagnetic simulations to model Permalloy based synthetic magnets that include both dipolar interactions, as well as the interlayer exchange coupling which determines whether or not the material is ferromagnetic or antiferromagnetic. For the material parameters considered in this work, we predict that only a single exceptional point is present when the system is ferromagnetic, and that no exceptional point appears when the material is antiferromagnetic. These results suggest that when calculating exceptional points within layered magnetic materials, interactions other than the interlayer exchange field must be accounted to accurately predict the existence of exceptional points, and that micromagnetic simulations are a useful tool to perform this task.

The increased attention toward antiferromagnets[1] (AFM), and their technological potential, frequently centers on studies involving AFM magnons. In antiferromagnets, long wavelength magnons can have frequencies in the GHz,[2] subterahertz,[3,4] and THz regime.[5,6] These higher frequencies are not usually accessible in ferromagnetic systems, except at large wavenumbers. Due to the presence of both optical and acoustic magnon branches within AFMs, and layered magnets, there are opportunities to use interactions between the magnon branches as a means to control the magnons. Layered magnetic materials, such as synthetic magnets and van der Waals magnets, are good platforms to test these ideas because both optical and acoustic magnons can exist in the GHz frequency range. This accessibility has enabled experiments and simulations that seek to control magnon-magnon interactions in layered magnets through the usage of symmetry-breaking external fields,[7,8] dipolar interactions,[9] and interlayer exchange fields.[10] These interactions can couple both acoustic and optical magnons, as well as optical and acoustic magnon pairs. Elucidating mechanisms that can control/manipulate magnon–magnon interactions is, at present, one of the general goals for designing devices based on hybridized quantum excitations.[11–13]

An alternative way to control the magnon spectrum in layered materials is through the use of exceptional points (EPs). In the context of layered magnets, EPs can be found in a pair of exchange coupled Landau–Lifshitz–Gilbert (LLG) equations, when each equation has a different magnetic damping parameter.[14–16] By changing material parameters within the LLG equations, such as the damping ratio between the two layers or the interlayer exchange field, EPs can be observed. Typically, an optical and acoustic magnon branch coalesce and merge into a single magnon branch at an EP.[14] Associated with this coalescence is a change in the character of the two eigenvalues describing the individual optical and acoustic magnons from real to complex numbers.[14–16] It is important to mention that the usage of EPs, in magnonic-based systems, extends far beyond layered materials. EPs are the subject of interest in hybrid quantum systems involving magnons and microwave photons,[17–19] and more recently in engineering new functionalities within magnonic waveguides.[20]

Over the last decade, EP phenomena in bulk magnetic systems have been more heavily investigated than the thin film systems discussed in this work. For example, the use of macroscopic yttrium iron garnet structures with rf cavities is an ideal platform for investigating fundamental physics in magnetic EP phenomena.[17–19,21] However, these large systems lack sufficient engineering approaches for device integration, including but not limited to, energy converters and sensors that take advantage of the EP physics. On the other hand, thin-film based, synthetic magnetic heterostructures are a promising platform for incorporating a wide variety of material engineering and structural design for practical device application purposes. This includes interfacial exchange interactions,[22] spin-orbital torques,[23,24] and local electric or magnetic field tuning with external current/voltage inputs.[25] These engineering approaches naturally connect the EP phenomena with engineering approaches that have been already available from modern CMOS technologies. Such perspective is also reinforced by the growing capability of nanofabrication and engineering of key magnonic materials such as YIG heterostructures.[26]

The magnonic systems we model in this work are synthetic magnets consisting of two ferromagnetic (FM) films separated by a nonmagnetic (NM) film.[2] An archetypal synthetic magnet is a trilayer in a FM/NM/FM configuration. By selecting spacer layers such as Ru and Pt, the Ruderman–Kittel–Kasuya–Yosida (RKKY) can couple the FM layers together in either a FM or AFM configuration.[27] The strength and sign of this interlayer interaction depend on the thickness of the NM layer. The LLG equations used to model synthetic magnets treat individual magnetic layers as two rigid magnetic moments (macrospins) that are coupled together via an exchange field.[14,15,28] For EPs to occur, the equations must have an asymmetry in the magnetic damping constants that are used; one macrospin must have a larger damping than the other. Once the equations are linearized, the eigenvalues that correspond to magnon frequencies are obtained through standard methods. The results of this analysis predict two exceptional points that can be found for both FM and AFM interlayer exchange fields. The exchange field values where the EPs occur share the same magnitude, i.e., they are symmetric about an exchange field of zero.[28]

In real synthetic magnets, the dipolar interaction causes the magnetic layers to have an AFM preference, even in the absence of an interlayer exchange interaction. Thus, we anticipated that macrospin models required a quantitative correction in predicting the location where EPs occur as a function of interlayer exchange interactions. In this work, we investigated this question using Mumax3, an open source, GPU accelerated, micromagnetic simulation platform.[29] Mumax3 accounts for dipolar interactions as well as realistic shape demagnetization effects that would be present in any magnetic micro/nanostructure. Our results indicate that the inclusion of the dipolar interaction, using material parameters that would describe a real synthetic magnet, dramatically alters where EPs can and cannot appear as a function of the interlayer interaction.

As illustrated in Fig. 1(a), our simulations consist of two magnetic layers with the same saturation magnetization M_s, and the same intralayer exchange stiffness A_{ex}. We use material parameters of Permalloy so that the individual magnetic layers had $M_s = 770 \times 10^3$ A/m and $A_{ex} = 13 \times 10^{-12}$ J/m. An interlayer exchange stiffness, of the order 10^{-16} J/m, between the two layers is treated as an independent variable that is different from the intralayer coupling. For our geometry, we considered an ellipse 160 nm in length and 80 nm wide. The

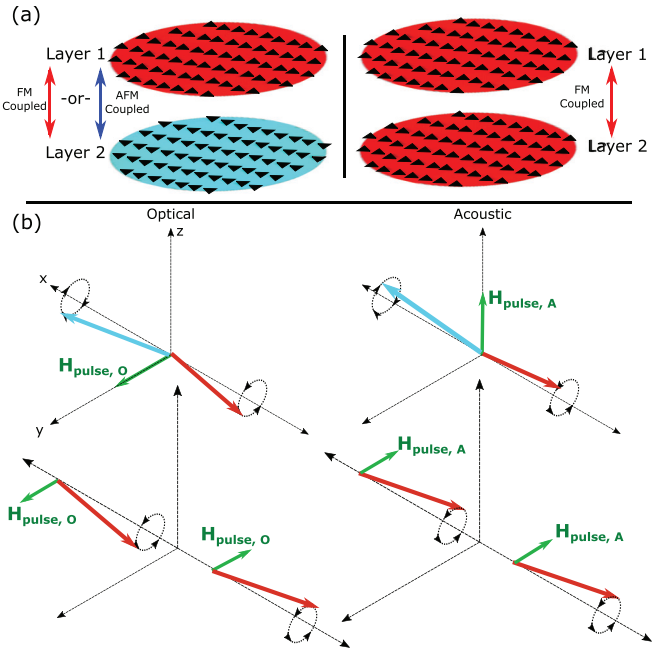

FIG. 1. (a) Illustration of two micromagnetic layers that are in an antiferromagnetic alignment yet can be coupled with either a FM or AFM interlayer interaction (left image). Also, two layers are shown in a ferromagnetic alignment with a FM interlayer interaction (right image). (b) Using red and teal arrows to represent the orientation of micromagnetic layers, we illustrate what the optical and acoustic magnon modes look like when the system is in either an AFM or FM alignment. The green arrows label field pulse directions that can be used in micromagnetic simulations to excite the corresponding modes.

micromagnetic cell size was chosen to be $1.25 \times 1.25 \times 0.6\,\text{nm}^3$. The interlayer exchange stiffness effectively models the strength and sign of the RKKY interaction. We considered both positive and negative signs in the interlayer exchange stiffness. Two magnetic damping parameters are needed to describe the bilayer; α_1 and α_2 represent the Landau Lifshitz damping parameter for the first and second layer, respectively. As known from macrospin models, for an EP to form the ratio of α_1/α_2 must differ from unity.[14,28] In our work, we fix $\alpha_1/\alpha_2 = 1/3$. We have tested more severe damping ratios ($\alpha_1/\alpha_2 = 1/10$), and our main conclusions are insensitive to the range that was considered. Experimentally, this damping ratio can be achieved by depositing a Pt "capping" layer over top of the final magnetic layer. Through the spin Hall effect, a dc electrical current can in principle be used to bias a device such that the top Permalloy layer experiences an (anti)damping-like torque[30] which effectively controls α_1/α_2.

In addition to setting up the relevant magnetic material parameters, care must be taken in considering the magnetic state of the synthetic magnet. Unlike macrospin models, the magnetic state does not just depend on whether the interlayer exchange interaction is FM or AFM. The dipolar interaction prefers an AFM alignment even if the interlayer exchange interaction is set to zero. Thus, for a range of small FM interlayer exchange interactions, a stable AFM state exists. An understanding of available magnetic states is important because the manner in which magnons are excited depends on the ground state [as illustrated in Fig. 1(b)]. First, consider an AFM ground state. To

excite optical magnons, a uniform field pulse in the y-direction is required, and a field pulse in either the x- or z-direction will excite acoustic magnons. Thus, when we excite optical and acoustic magnons within an AFM ground state, unless otherwise specified, we use a spatially uniform field pulse that has a strength of 3 mT y-direction and 3 mT in both the x- and z-direction. If the magnet has a FM ground state, the acoustic magnons can be excited with a spatially uniform pulse in either the x- or z-direction, and the optical modes can be excited by a spatially *nonuniform* pulse in the y-direction that changes polarity depending on the layer. When exciting a superposition of acoustic and optical FM magnons we use a field pulse that has a strength of 3 mT and -3 mT in the y-direction of first and second layers, respectively. In addition, the pulse has a spatially uniform component of 3 mT in both the x- and z-direction.

Aside from how the field pulse is shaped, the simulations run identical for a FM or an AFM state. First, the two layers are initialized in either a FM or AFM alignment and relaxed into a magnetostatic equilibrium configuration. Next, the field pulse is applied for a duration of 100 ps. The pulse is then turned off, and the system is time-evolved for an additional 10 ns. Throughout this process, the average magnetization of both layers is recorded as a time series with a sampling period of 10 ps. To obtain the magnon energy spectrum, we take a fast Fourier transform (FFT) of the time series that describes either layer. We take the FFT with respect to the y-component of the magnetization (an in-plane component), or the z-component of the magnetization (the out-of-plane component). This process is then repeated for different interlayer exchange values.

We first consider EPs when the state of the synthetic magnet is ferromagnetic. In Fig. 2, results are shown for a FM interlayer exchange interaction in a range between $0.75–3 \times 10^{-16}$ J/m. In panels (a) and (c), we calculate spectra by taking the FFT of the out-of-plane component of the magnetization averaged between layers as well as a FFT of an individual layer. This allows us to better identify the acoustic magnon branch in the former, and the optical branch in the latter. For larger interlayer exchange values we observe an acoustic branch near 3.4 GHz, and an optical branch that depends on the value of the interlayer exchange interaction. The optical branch and the acoustic branch are shown to intersect when the interlayer exchange interaction is 1.6×10^{-16} J/m. For interlayer exchange stiffness values that are smaller than this critical value, the "flat" acoustic branch is strongly attenuated. This attenuation is also visualized in panels (b) and (d), where representative individual magnon spectra are shown for exchange stiffness values above, at, and below the EP. The coalescence of the two magnon branches, combined with the suppression of one magnon branch after coalescence occurs, is interpreted as an EP in the ferromagnetic interlayer exchange coupling parameter space. To further verify that the suppression of the acoustic branch represents an EP, in Figs. 3(a) and 3(b), we repeat the simulation with $\alpha_1/\alpha_2 = 1$, taking the FFT of the averaged layers and a single layer in the same manner as Fig. 2. Very clearly, there is no extermination of the acoustic branch, and both the optical and acoustic branches are permitted to exist over the entire range of exchange stiffness values considered. In summation, when compared with macrospin models, our results for the synthetic FM configuration are in qualitative agreement. An EP is observed when both the magnetic state as well as the interlayer exchange stiffness are ferromagnetic.

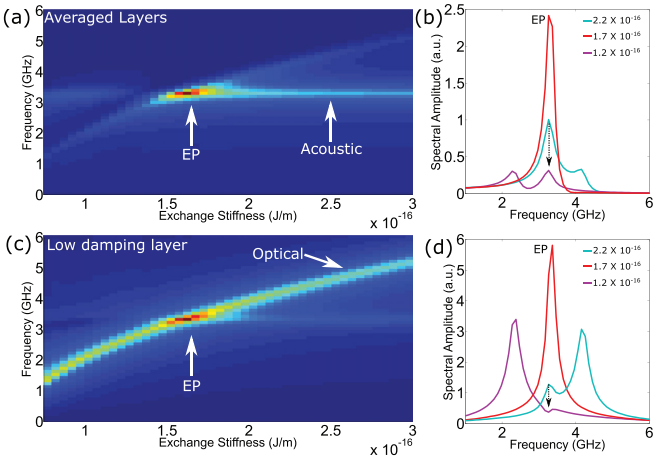

FIG. 2. Here we consider the case where $\alpha_1/\alpha_2 = 1/3$ for the synthetic ferromagnet. (a) The magnon spectra for both optical and acoustic branches are shown when an FFT is taken of the averaged out-of-plane component of the magnetization between both layers, which better visualizes the acoustic branch. For exchange stiffness values that fall below the EP, the acoustic branch is suppressed. (b) Individual spectra from the color map in (a) are shown for an exchange stiffness above, at, and below the EP. Above and below the EP, the optical mode has a similar amplitude. Below the EP, the acoustic branch is suppressed. At the EP, there is an enhancement in the amplitude when the branches overlap. (c) The magnon spectra for both optical and acoustic branches are shown when an FFT is taken of the averaged out-of-plane component of an individual layer (the low damping layer). In this spectra, the optical branch more visible. (d) Individual spectra from the color map in (c) are shown for an exchange stiffness above, at, and below the EP. Again, as the black arrow indicates, the acoustic mode is suppressed below the EP. The optical mode is seen to increase in amplitude below the EP.

We now discuss our results when the state of the synthetic magnetic is antiferromagnetic. Using an AFM interlayer exchange stiffness in a range from -3×10^{-16}–0 J/m, we consider a parameter space that is symmetric with respect to the range used for the synthetic ferromagnet. As shown in Fig. 4(a), both the optical and acoustic magnon branches are excited. However, throughout this entire range of exchange stiffness values, there is never a crossing between the optical and acoustic branches. Even when the exchange stiffness is reduced to zero, and the AFM interaction is disabled, a gap of 3.3 GHz exists

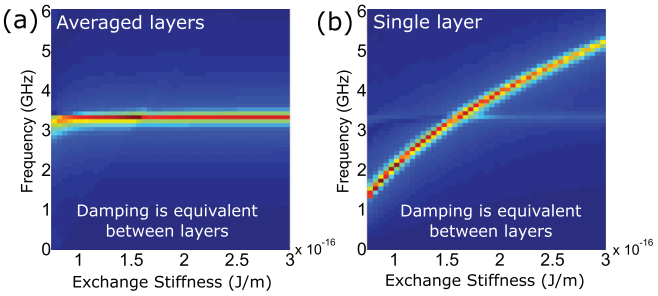

FIG. 3. (a) and (b) Here we consider the case where $\alpha_1/\alpha_2 = 1$ for the synthetic ferromagnet. The magnon spectra are shown when an FFT is taken of the out-of-plane components of the magnetization of the layers averaged together, or of an individual layer, respectively. The acoustic mode is visible throughout the parameter space in (a) and the optical mode is visible throughout the parameter space in (b).

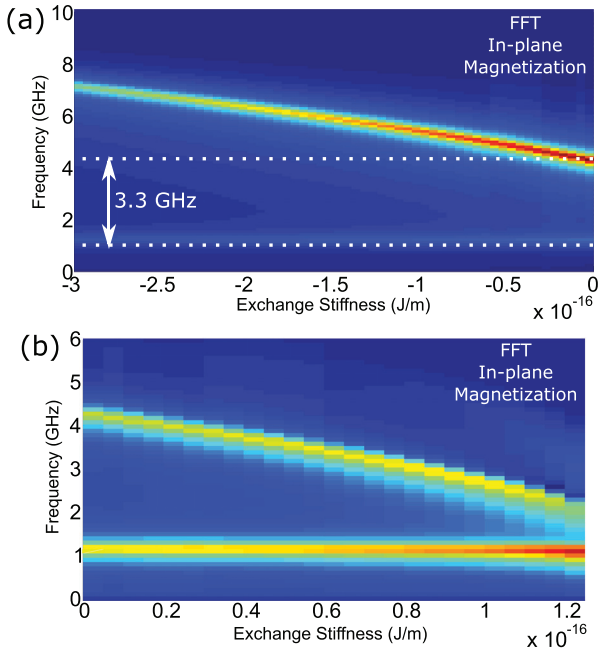

FIG. 4. (a) The magnon spectra are shown when taking an FFT of the in-plane component of the magnetization for an antiferromagnetic state when the interlayer exchange stiffness is AFM. No crossing between the optical and acoustic branch is observed. (b) The magnon spectra are shown when the antiferromagnetic state is stable with a FM interlayer exchange stiffness. For this simulation, we changed the orientation of the field pulse to more equally excite both the optical and acoustic branches. The field pulse is 10, 3, and 20 mT in the x-, y-, and z-direction, respectively. In this range of the parameter space, no clear evidence for an EP is found. The magnon branches start to intersect near 1.3×10^{-16} J/m, just as the antiferromagnetic state becomes unstable due to the FM exchange interaction.

between the optical and acoustic magnon branches. In other words, there is no observed EP when the interlayer exchange coupling is antiferromagnetic in nature. This is in direct contrast to macrospin models, which predict an EP exists when the interlayer exchange field is AFM.

Due to the dipolar interaction, an antiferromagnetic state is stable even for a range of interlayer exchange stiffness values that are ferromagnetic. A natural question then arises: Does a second EP exist in the phase space where the interlayer exchange stiffness is ferromagnetic, yet the magnetic state is antiferromagnetic? To answer this question, we performed additional simulations for a range of FM interlayer exchange stiffness values between 0 and 1.3×10^{-16} J/m. If the FM interlayer exchange interaction is increased above this upper limit the AFM ground state is no longer stable, and nonlinear magnetization dynamics are excited via our field pulse. For the material parameters selected in this work, no EP is reached in this parameter space. In Fig. 4(b), we show the FFT with respect to the time series of the averaged in-plane component of the magnetization. The magnon branches are just starting to coalesce as just as the AFM ground state destabilizes when the exchange stiffness is equal to 1.3×10^{-16} J/m. Thus, we never observe the strong attenuation of a magnon branch like the FM counterpart. We conclude that for the material parameters considered in this work, *synthetic antiferromagnets will not be guaranteed to have an EP due to dipolar interactions.*

In this Letter, we have examined the coalescence of "quasi-uniform" optical and acoustic magnons in a micromagnetic simulation structure. These simulations are a useful, and necessary, companion to the macrospin models predominantly used to model EPs in magnonic systems. By designing the simulation with a nanomagnet having a negligible spacer layer thickness, our simulations are a limiting case where the dipolar interaction is impactful. Macrospin models represent the other limiting case and are more valid for continuous thin films. Future work that examines both spacer layer thicknesses, as well as the size of the micromagnetic objects, will serve as a bridge between these two limiting cases. In the case of our simulations, the dipolar interaction does not qualitatively generate different physical effects when both the magnetic state and interlayer exchange interaction are ferromagnetic. However, for a Permalloy/Ru-based synthetic AFM structure, we predict that no EP exists if the interlayer coupling is antiferromagnetic. It also appears that the system is approaching, but not reaching, a second EP when there is an antiferromagnetic ground state with a ferromagnetic coupling. For the material parameters we have considered, these results indicate that micromagnetic simulations are a necessary refinement over macrospin models when predicting the location of exceptional points in synthetic magnets.

Work at Oakland University was supported by U.S. National Science Foundation under Award No. ECCS-1941426.

DATA AVAILABILITY

The data that support the findings of this study are available from the corresponding author upon reasonable request.

REFERENCES

[1]S. A. Siddiqui, J. Sklenar, K. Kang, M. J. Gilbert, A. Schleife, N. Mason, and A. Hoffmann, "Metallic antiferromagnets," J. Appl. Phys. **128**, 040904 (2020).
[2]H. Waring, N. Johansson, I. Vera-Marun, and T. Thomson, "Zero-field optic mode beyond 20 GHz in a synthetic antiferromagnet," Phys. Rev. Appl. **13**, 034035 (2020).
[3]J. Li, C. B. Wilson, R. Cheng *et al.*, "Spin current from sub-terahertz-generated antiferromagnetic magnons," Nature **578**, 70–74 (2020).
[4]P. Vaidya, S. A. Morley, J. van Tol, Y. Liu, R. Cheng, A. Brataas, D. Lederman, and E. D. Barco, "Subterahertz spin pumping from an insulating antiferromagnet," Science **368**, 160–165 (2020).
[5]T. Moriyama, K. Hayashi, K. Yamada, M. Shima, Y. Ohya, and T. Ono, "Intrinsic and extrinsic antiferromagnetic damping in NiO," Phys. Rev. Mater. **3**, 051402 (2019).
[6]T. Moriyama, K. Hayashi, K. Yamada, M. Shima, Y. Ohya, and T. Ono, "Tailoring THz antiferromagnetic resonance of NiO by cation substitution," Phys. Rev. Mater. **4**, 074402 (2020).
[7]D. MacNeill, J. T. Hou, D. R. Klein, P. Zhang, P. Jarillo-Herrero, and L. Liu, "Gigahertz frequency antiferromagnetic resonance and strong magnon-magnon coupling in the layered crystal $CrCl_3$," Phys. Rev. Lett. **123**, 047204 (2019).
[8]A. Sud, C. Zollitsch, A. Kamimaki, T. Dion, S. Khan, S. Iihama, S. Mizukami, and H. Kurebayashi, "Tunable magnon-magnon coupling in synthetic antiferromagnets," Phys. Rev. B **102**, 100403 (2020).
[9]Y. Shiota, T. Taniguchi, M. Ishibashi, T. Moriyama, and T. Ono, "Tunable magnon-magnon coupling mediated by dynamic dipolar interaction in synthetic antiferromagnets," Phys. Rev. Lett. **125**, 017203 (2020).
[10]J. Sklenar and W. Zhang, "Self-hybridization and tunable magnon-magnon coupling in van der waals synthetic magnets," Phys. Rev. Appl. **15**, 044008 (2021).
[11]Y. Li, W. Zhang, V. Tyberkevych, W.-K. Kwok, A. Hoffmann, and V. Novosad, "Hybrid magnonics: Physics, circuits, and applications for coherent information processing," J. Appl. Phys. **128**, 130902 (2020).

[12]D. Awschalom, C. Du, R. He *et al.*, "Quantum engineering with hybrid magnonics systems and materials," preprint arXiv:2102.03222 (2021).
[13]Y. Xiong, Y. Li, M. Hammami *et al.*, "Probing magnon–magnon coupling in exchange coupled $Y_3Fe_5O_{12}$/permalloy bilayers with magneto-optical effects," NPG Sci. Rep. **10**, 12548 (2020).
[14]J. Lee, T. Kottos, and B. Shapiro, "Macroscopic magnetic structures with balanced gain and loss," Phys. Rev. B **91**, 094416 (2015).
[15]A. Galda and V. M. Vinokur, "Parity-time symmetry breaking in magnetic systems," Phys. Rev. B **94**, 020408 (2016).
[16]T. Yu, H. Yang, L. Song, P. Yan, and Y. Cao, "Higher-order exceptional points in ferromagnetic trilayers," Phys. Rev. B **101**, 144414 (2020).
[17]D. Zhang, X.-Q. Luo, Y.-P. Wang, T.-F. Li, and J. You, "Observation of the exceptional point in cavity magnon-polaritons," Nat. Commun. **8**, 1–6 (2017).
[18]X. Zhang, K. Ding, X. Zhou, J. Xu, and D. Jin, "Experimental observation of an exceptional surface in synthetic dimensions with magnon polaritons," Phys. Rev. Lett. **123**, 237202 (2019).
[19]J. Zhao, Y. Liu, L. Wu, C.-K. Duan, Y.-X. Liu, and J. Du, "Observation of anti-PT-symmetry phase transition in the magnon-cavity-magnon coupled system," Phys. Rev. Appl. **13**, 014053 (2020).
[20]X.-G. Wang, G.-H. Guo, and J. Berakdar, "Steering magnonic dynamics and permeability at exceptional points in a parity–time symmetric waveguide," Nat. Commun. **11**, 1–8 (2020).
[21]Y. Yang, Y.-P. Wang, J. Rao, Y. Gui, B. Yao, W. Lu, and C.-M. Hu, "Unconventional singularity in anti-parity-time symmetric cavity magnonics," Phys. Rev. Lett. **125**, 147202 (2020).
[22]A. Fernández-Pacheco, E. Vedmedenko, F. Ummelen, R. Mansell, D. Petit, and R. P. Cowburn, "Symmetry-breaking interlayer dzyaloshinskii–moriya interactions in synthetic antiferromagnets," Nat. Mater. **18**, 679–684 (2019).
[23]P. Zhang, L. Liao, G. Shi, R. Zhang, H. Wu, Y. Wang, F. Pan, and C. Song, "Spin-orbit torque in a completely compensated synthetic antiferromagnet," Phys. Rev. B **97**, 214403 (2018).
[24]C. Bi, H. Almasi, K. Price, T. Newhouse-Illige, M. Xu, S. R. Allen, X. Fan, and W. Wang, "Anomalous spin-orbit torque switching in synthetic antiferromagnets," Phys. Rev. B **95**, 104434 (2017).
[25]Q. Yang, L. Wang, Z. Zhou *et al.*, "Ionic liquid gating control of RKKY interaction in FeCoB/Ru/FeCoB and $(Pt/Co)_2/Ru/(Co/Pt)_2$ multilayers," Nat. Commun. **9**, 1–11 (2018).
[26]S. Li, W. Zhang, J. Ding, J. E. Pearson, V. Novosad, and A. Hoffmann, "Epitaxial patterning of nanometer-thick $Y_3Fe_5O_{12}$ films with low magnetic damping," Nanoscale **8**, 388–394 (2016).
[27]R. Duine, K.-J. Lee, S. S. Parkin, and M. D. Stiles, "Synthetic antiferromagnetic spintronics," Nat. Phys. **14**, 217–219 (2018).
[28]H. Liu, D. Sun, C. Zhang, M. Groesbeck, R. Mclaughlin, and Z. V. Vardeny, "Observation of exceptional points in magnonic parity-time symmetry devices," Sci. Adv. **5**, eaax9144 (2019).
[29]A. Vansteenkiste, J. Leliaert, M. Dvornik, M. Helsen, F. Garcia-Sanchez, and B. Van Waeyenberge, "The design and verification of MuMax3," AIP Adv. **4**, 107133 (2014).
[30]J. Sklenar, W. Zhang, M. B. Jungfleisch, H. Saglam, S. Grudichak, W. Jiang, J. E. Pearson, J. B. Ketterson, and A. Hoffmann, "Unidirectional spin-torque driven magnetization dynamics," Phys. Rev. B **95**, 224431 (2017).